Niemelä, Janne-Petteri; Giri, A.; Hopkins, P.E.; Karppinen, Maarit

Ultra-low thermal conductivity in TiO2:C superlattices

Published in:
JOURNAL OF MATERIALS CHEMISTRY. A

DOI:
10.1039/C5TA01719J

Published: 01/01/2015

Document Version
Peer-reviewed accepted author manuscript, also known as Final accepted manuscript or Post-print

Please cite the original version:
Niemelä, J.-P., Giri, A., Hopkins, P. E., & Karppinen, M. (2015). Ultra-low thermal conductivity in TiO2:C superlattices. *JOURNAL OF MATERIALS CHEMISTRY. A*, *2015*(3), 11527-11532. https://doi.org/10.1039/C5TA01719J

Journal of Materials Chemistry A RSCPublishing

PAPER

Ultra-low thermal conductivity in TiO_2:C superlattices

Cite this: DOI: 10.1039/x0xx00000x

Janne-Petteri Niemelä[1], Ashutosh Giri[2], Patrick E. Hopkins[2] and Maarit Karppinen[1]

Received 00th January 2012,
Accepted 00th January 2012

DOI: 10.1039/x0xx00000x

www.rsc.org/

TiO_2:C superlattices are fabricated from atomic/molecular layer deposited (ALD/MLD) inorganic-organic $[(TiO_2)_m(Ti\text{-}O\text{-}C_6H_4\text{-}O\text{-})_{k=1}]_n$ thin films via a post-deposition annealing treatment that converts the as-deposited monomolecular organic layers into sub-nanometer-thick graphitic interface layers confined within the TiO_2 matrix. The internal graphitic layers act as effective phonon-scattering boundaries that bring about a ten-fold reduction in thermal conductivity of the films with decreasing superlattice period down to an ultra-low value of 0.66±0.04 $Wm^{-1}K^{-1}$ – a finding that makes inorganic-C superlattices fabricated with the present method as promising structures for *e.g.* high-temperature thermal barriers and thermoelectrics.

Introduction

Materials with ultra-low thermal conductivity are needed, *e.g.*, for thermal-barrier and thermoelectric applications; the latter application calls for novel heavily-doped semiconductors able to combine thermal insulation with high electronic conductivity and thermopower. General pathways to suppress thermal transport in fully-dense solid materials exploit the introduction of structural disorder in the form of, *e.g.*, point defects, alloying components, amorphous phases, grain boundaries or material interfaces. Both experiments and theory have shown that the introduction of material interfaces is particularly well harnessed in various superlattice and multilayer thin-film materials where the interfaces between alternating layers of dissimilar materials act as phonon-scattering boundaries: not only may thermal conductivity be suppressed by an order of magnitude across the film plane[1-2] but a significant drop may also be seen in the in-plane direction.[3-4] Furthermore, careful balancing between order and disorder in multilayers may enable achieving ultra-low thermal conductivities comparable to or even lower than those of amorphous or porous materials, as evidenced by the results for, *e.g.*, W/Al_2O_3 nanolaminates (~0.6 $Wm^{-1}K^{-1}$) and layered WSe_2 crystals (~0.05 $Wm^{-1}K^{-1}$).[5-7]

For small-period superlattices the dominance of the phonon-boundary scattering at the internal interfaces over the scattering by the bulk of the constituent materials enables the control of thermal conductivity through careful adjustment of the superlattice period;[8] efficient suppression is achieved for incoherent phonons by decreasing the period, until potentially, phonon coherence may yield an upturn for periods similar to (and smaller than) phonon mean free path.[9-10] However, control over thermal conductivity in layered materials is not limited to simple size effects, as in particular for inorganic-organic materials, the drastic mismatch of the vibrational properties and the control over the bond strength over the internal interfaces may allow for further suppression of phonon transport.[11-12] Regarding inorganic-organic materials, use of organic layers of proper thicknesses could also allow for exploitation of phonon filtering realized due to interference effects within the organic layer.[13] In particular, a further degree of freedom to material design is brought about by the fact that use of carbon in fabrication of inorganic-organic interfaces is not limited to molecular organic layers, as interestingly also van-der-Waals bonded graphene interlayers have been demonstrated to have a lowering effect on thermal boundary conductance.[14-15]

An intriguing route for mixing inorganics and organics with highly dissimilar properties in a controlled manner is to employ atomic layer deposition (ALD) and molecular layer deposition (MLD) techniques in combination (ALD/MLD).[16] Besides simple homogeneous hybrid thin-film materials, such a combinatorial approach enables one to fabricate inorganic-organic superlattices with atomic/molecular monolayer precision via self-limiting surface reactions.[17-19] The self-limited film growth moreover allows for conformal coating of nanostructures, the key requirement for many future applications.[20-21] Recently, notably low thermal conductivity values were realized for ZnO-based ALD/MLD-fabricated hybrid structures obtained *via* incorporation of molecular organic layers; this observation has arisen great interest in thermal properties of ALD/MLD hybrid thin films – in particular for low-temperature thermal-barrier and thermoelectric applications.[22,23]

Titanium dioxide is an n-type semiconductor generally known for its photocatalytic properties. However, the recent discovery of high electronic conductivity for heavily Nb-doped anatase thin films has directed increasing attention towards the transport properties - including thermoelectric properties - of TiO_2.[24,25] In this paper we demonstrate that ultra-low thermal conductivity values can be achieved in high-temperature-tolerant electronically conducting $[(TiO_2)_mC_{k=1}]_n$ superlattice thin films by harnessing phonon-boundary scattering at the sub-nanometer-thick graphitic internal-interfaces, and that such

interlayers can be formed from monomolecular-thick hydroquinone-based organic layers through a reductive annealing treatment of $[(TiO_2)_m(Ti\text{-}O\text{-}C_6H_4\text{-}O\text{-})_{k=1}]_n$ films grown with the ALD/MLD technique. Furthermore, we show that an incremental decrease in the thermal conductivity values is reached by addition of Nb point-defects into the TiO_2 matrix.

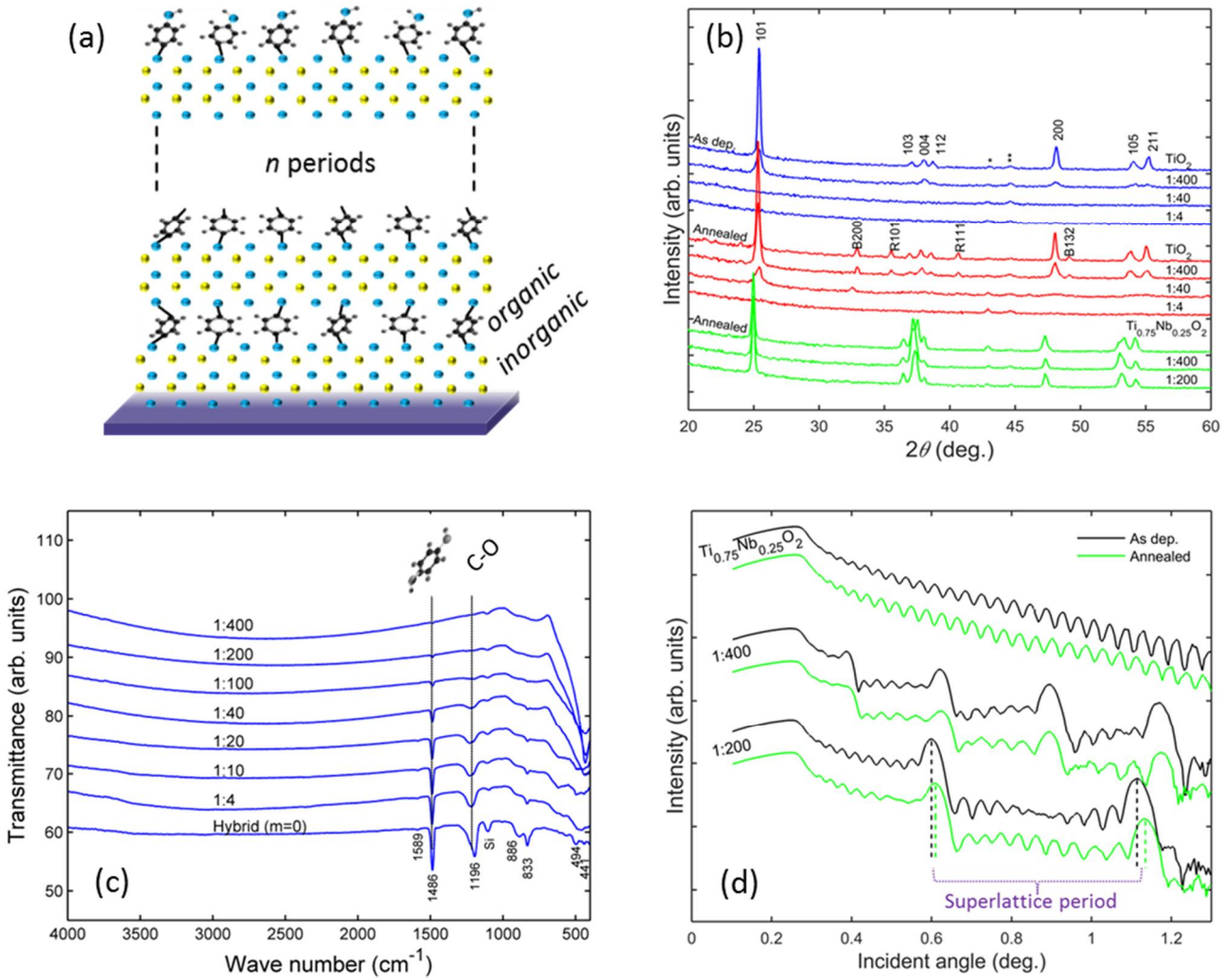

Figure 1. (a) An illustration of the $[(Ti_{1-x}Nb_xO_2)_m(Ti\text{-}O\text{-}C_6H_4\text{-}O\text{-})_{k=1}]_n$ superlattice structures with single layers of the $(Ti\text{-}O\text{-}C_6H_4\text{-}O\text{-})_{k=1}$ hybrid between octahedrally-coordinated $Ti_{1-x}Nb_xO_2$ (x = 0 or 0.25) layers. **(b)** GIXRD patterns for the superlattices with the main peaks indexed to the anatase structure of TiO_2, small impurities to the rutile (R) and brookite (B) structure and the tiny modulatios * to MgO substrate and ** to the substrate holder. **(c)** FTIR spectra for the films with x = 0 and k:m in the range of 1:400-1:4 and for (m=0) hybrid. **(d)** XRR patterns for the films with x = 0.25 and k:m ratio of 1:400 and 1:200, as well as for the purely inorganic $Ti_{0.75}Nb_{0.25}O_2$ film. The GIXRD and XRR results are shown for both as-deposited (As dep.) films and for the films obtained via annealing in Ar/H_2 gas at 600 °C.

Experimental

We fabricated a series of ~100 nm thick $[(TiO_2)_m(Ti\text{-}O\text{-}C_6H_4\text{-}O\text{-})_{k=1}]_n$ superlattice thin films on MgO and Si substrates at 210 °C *via* the ALD/MLD route described in detail previously.[19] In brief, the fabrication route consisted of alternate chemisorption of the precursor vapors of $TiCl_4$ (0.2 s), H_2O (0.1 s) and hydroquinone (HQ) (15 s) onto the substrate surface; N_2 was used as the carrier gas to transport the precursor vapors into the ALD reactor (Picosun R100), and as a purging gas, that removes any unreacted precursor molecules after each precursor pulse. To deposit a superlattice with n periods, a set of m alternate pulses of $TiCl_4$ and H_2O followed by one (k=1) cycle of the $TiCl_4$ and HQ precursors were repeated n times. Niobium-substituted superlattice films with the composition of $[(Ti_{0.75}Nb_{0.25}O_2)_m(Ti\text{-}O\text{-}C_6H_4\text{-}O\text{-})_{k=1}]_n$ were fabricated by

replacing every fourth $TiCl_4$ pulse for the TiO_2 block by a $Nb(OEt)_5$ (1 s) exposure.[26] An illustration of the targeted superlattice structures is show in Fig. 1 (a).

In order to determine the crystal structure of the thin films materials, grazing incidence x-ray diffraction technique (GIXRD; PANanalytical X'Pert Pro MPD diffractometer, Cu K_α) was employed; for x-ray reflectivity (XRR) studies the same instrument was operated in the reflection mode, and the obtained XRR patterns provided us with information for determination of the fim thicknesses and for the verification of the superlattice structures, *i.e.*, that well defined internal interface structures were indeed formed. Fourier transform infrared spectroscopy (FTIR; Nicolet magma 750 spectrometer) was utilized in determination of the chemical state of the inorganic-organic films – in particular, to verify the incorporation of the organic component (HQ) into the film structure.

The as-deposited films with molecular HQ-based organic layers were subjected to a strongly reductive post-deposition annealing – (Nabertherm GmbH RS 80/500/11) at 600 °C for 6 h in a tube furnace with flowing 5% H_2/Ar mixture (VARIGON® H5) as a reductive gas – in order to convert the molecular component into graphitic carbon. The carbon content of the annealed films was studied by means Raman spectroscopy (Thermo Fisher Scientific DXR-Raman microscope, 532 nm laser) and a subsequent fitting procedure was applied to the data, described more in detail in the results and discussion section, to enable a more-in-depth discussion.

The cross-plane thermal conductivity values were obtained *via* time-domain thermoreflectance (TDTR) – a technique that uses a combination of laser pulses to reveal the thermal properties of the sample: first, pump pulses introduce a stimulus of thermal energy to a metal transducer (here Al) on the sample surface, and second, probe pulses detect the consequent change in reflectance determined by the thermal properties of the sample.[27-29]

Results and discussion

The as-deposited TiO_2 film crystallizes with the anatase structure as is evidenced by GIXRD studies (Figure 1 (b)). However, the introduction of the organic layers suppresses the crystallinity of the superlattice films in a way that for k:$m \leq$ 1:200 the films are amorphous. The as-deposited Nb-substituted superlattice films are amorphous, as a consequence of the amorphous character of the $Ti_{0.75}Nb_{0.25}O_2$ matrix. The aromatic rings from the HQ precursor molecules are delivered to the structure intact as the FTIR spectra show a prominent absorption peak at around 1486 cm^{-1} corresponding to the C=C stretching in the aromatic rings from the HQ precursor and a weak aromatic ring signal at 1589 cm^{-1} (Fig. 1 (c)). We also see a broad C-O stretching signal at around 1196 cm^{-1} indicating that the molecular monolayers of the aromatic rings readily bond via oxygen atoms to the inorganic matrix. Furthermore, the XRR reflectograms show well-defined constructive interference patterns stemming from the molecular layers – a fact that confirms the formation of the targeted superlattice structures with single-molecular layers periodically sandwiched between the wider inorganic layers (Fig. 1 (d)).

In an attempt to transform the molecular HQ-based organic layers in the as-deposited films into graphitic carbon layers, the films were subjected to a strongly reductive post-deposition annealing; as a result the crystallinity of the films is notably enhanced such that even the $[(TiO_2)_m(Ti\text{-}O\text{-}C_6H_4\text{-}O\text{-})_{k=1}]_n$ film with k:m of 1:40 yields moderate reflections. During the annealing step minor impurities of the rutile and the brookite structures of TiO_2 form within the anatase matrix, which is prevented by Nb-substitution. Note that Nb indeed substitutes Ti in the structure, as the anatase peaks are seen to shift towards lower angles as a sign of increasing unit cell volume (Fig. 1 (b)). Given the high annealing temperature, it is remarkable that the annealing treatment retains the internal interfaces of the superlattice structure as is effectively verified from the XRR patterns shown in Fig. 1 (d). The very small difference between the patterns for the as-deposited and the annealed films, i.e., the fine widening of the fringes (compare the superlattice periods for the 1:200 sample marked with the dashed lines in Fig. 1 (d)) can be ascribed to the increased film density and hence reduced film thickness due to both the improved crystallinity of the inorganic matrix and the probable contraction of the organic layers.

To get more insight into the carbon content in the fine internal interface layers of our annealed superlattice films, we studied the films by means of Raman spectroscopy. The results are shown in Fig. 2 in the wave number range of 1050 – 3000 cm^{-1} for the Nb-doped films, denoted now as $[(Ti_{0.75}Nb_{0.25}O_2)_mC_{k=1}]_n$: the spectra show prominent peaks for sp^2 carbon at 1338 cm^{-1} and 1602 cm^{-1}, typically labeled as disordered D and graphitic G, respectively, and a modulated bump between 2400 and 3000 cm^{-1} consisting of second-order peaks of D peak overtone G' and the combination mode D + G.[30-31] The D peak is a breathing mode of A_{1g} symmetry with its intensity strictly connected to the presence of six-fold aromatic rings; the mode is forbidden in perfect graphite and only becomes active in the presence of disorder. The G peak stems from bond-stretching motion of pairs of carbon atoms both in rings and chains, and has E_{2g} symmetry. We fitted the spectral range of the D and G peaks using a Lorentzian for the D peak and a Breit-Wigner-Fano distribution for the G peak (inset of Figure 2) in order to further evaluate the carbon content in our films. Based on the model of Ferrari and Robertson,[30] the maximally high G position of 1602 cm^{-1} indicates the carbon layers in our films to have nanocrystalline nature. The ratio for integrated intensities yields $A(D)/A(G) \approx 1.7$, whereas for the comparison of the peak heights a value $I(D)/I(G) \approx 0.7$ is obtained. Supposing that the comparison of the areas A(D)/A(G) gives proper information, the picture with nanocrystalline graphite is supported. However, as a sign of a degree of amorphousness and disorder, the D peak is found markedly broader in comparison to the G peak. As for amorphous carbon the information on the less distorted rings should be better reflected in the height of the D peak, rather than in its area, I(D)/I(G) comparison could be justified. According to ref. 30 the value $I(D)/I(G) \approx 0.7$ should anyhow coexist with notably lower G position value than 1602 cm^{-1} – a consideration that leaves us with an ambiguity. In the end, in accordance with ref. 32, the carbon layers in our annealed superlattice thin films are probably best described as a mixture of nanocrystalline graphite and amorphous carbon, as crystallinity is seen in the high G position value and amorphous character in the broadening of the D peak.

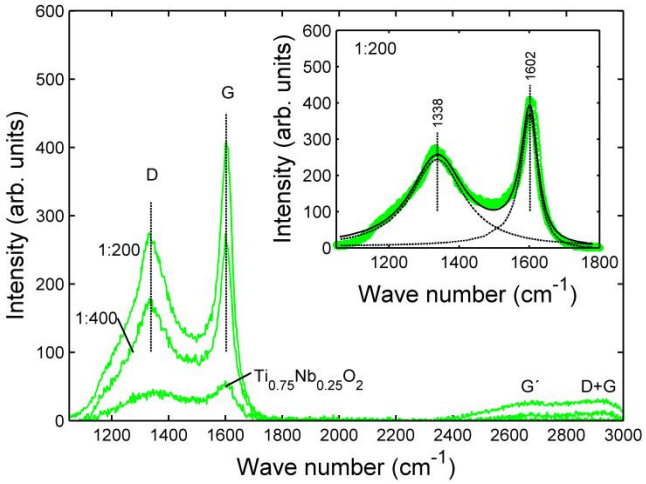

Figure 2 Raman spectra for the $[(Ti_{0.75}Nb_{0.25}O_2)_mC_{k=1}]_n$ thin films for *k*:*m* ratios 1:400 and 1:200, as well as for the purely inorganic $Ti_{0.75}Nb_{0.25}O_2$ film, obtained via annealing in Ar/H_2 gas at 600 °C. The inset shows fitting of the D and the G peak using a Lorentzian for the D peak and a Breit-Wigner-Fano distribution for the G peak.

The present inorganic-organic interfaces enable a marked suppression of heat transport in the present inorganic-organic superlattices, as was verified by means of the TDTR technique. In Fig. 3 we show the results for cross-plane thermal conductivities κ determined from the TDTR data for both the as-deposited superlattice thin films with molecular aromatic carbon layers and for the annealed superlattice films with graphitic carbon layers. The annealed TiO_2 film has κ of 6.78±0.40 $Wm^{-1}K^{-1}$, in good agreement with the literature value of ~6 $Wm^{-1}K^{-1}$ for anatase TiO_2 thin films.[33] In comparison to the purely inorganic TiO_2 films, graphitic carbon layers in the $[(TiO_2)_mC_{k=1}]_n$ superlattices markedly decrease the κ values down to 3.79±0.30, 1.49±0.10 and 0.66±0.04 $Wm^{-1}K^{-1}$ for *k*:*m* ratios of 1:400, 1:40 and 1:4, respectively; note that the overall decrease is as large as ten-fold and that the minimum lies greatly below the amorphous limit for TiO_2 measured here as 1.33±0.10 $Wm^{-1}K^{-1}$. For purely inorganic TiO_2, addition of Nb point-defects as phonon scattering centers reduces κ to 3.49 ±0.30 $Wm^{-1}K^{-1}$ for the $Ti_{0.75}Nb_{0.25}O_2$ film. An incremental decrease of κ is seen for the $[(Ti_{0.75}Nb_{0.25}O_2)_mC_{k=1}]_n$ superlattices via introduction of the graphitic layers, as the κ value for the film with *k*:*m* of 1:400 is found as low as 1.68±0.15 $Wm^{-1}K^{-1}$. The fact that the thermal conductivity values decrease with decreasing superlattice period indicates that cross-plane thermal transport through the superlattices is predominately suppressed by incoherent boundary scattering of phonons.[9-10] Such is valid as the heat transport here is indeed phonon dominated, as for the $[(TiO_2)_mC_{k=1}]_n$ superlattices with electronic resistivity around 1×10^{-1} Ωm, the Wiedemann-Franz law $\kappa_e = L\rho^{-1}T$, where L (=2.45×10^{-8} $W\Omega K^{-2}$) is the Lorentz number, ρ electronic resistivity and T temperature, yields neligible contribution for electrons of $\kappa_e/\kappa \approx 7\times10^{-3}$ at room temperature. Thermal conductivity for the Nb-doped films is phonon dominated, though, electrons do contribute moderately: the resistivity values for the $Ti_{0.75}Nb_{0.25}O_2$ and the respective *k*:*m* = 1:400 superlattice were measured as 2.7×10^{-3} Ωm and 1.2×10^{-3} Ωm that yield ratios $\kappa_e/\kappa \approx 0.08$ and $\kappa_e/\kappa \approx 0.36$, hence confirming the fact that the reduction in thermal conductivity is due to increased phonon scattering. Note that the present $[(Ti_{1-x}Nb_xO_2)_mC_{k=1}]_n$ superlattice structures are stable at high temperatures of at least 600 °C – a fact that makes these structures particularly interesting for high-temperature applications.

The thermal conductivity values for the as-deposited superlattices show similar decreasing trend with decreasing superlattice period as was observed for the annealed ones. Overall, the κ values for the $[(TiO_2)_m(Ti\text{-}O\text{-}C_6H_4\text{-}O\text{-})_{k=1}]_n$ films are slightly lower than those for the $[(TiO_2)_mC_{k=1}]_n$ films, which can most likely be ascribed to improved crystallinity upon the annealing treatment, and indeed the lowest κ value among the present sample series, *i.e.*, 0.62±0.04 $Wm^{-1}K^{-1}$ is found for the as-deposited $[(TiO_2)_m(Ti\text{-}O\text{-}C_6H_4\text{-}O\text{-})_{k=1}]_n$ superlattice film with *k*:*m* of 1:4. The as-deposited films have very high electronic resistance and consequently electrons do not give an important contribution to the heat transport. The results for the as-deposited $[(TiO_2)_m(Ti\text{-}O\text{-}C_6H_4\text{-}O\text{-})_{k=1}]_n$ films confirm the efficient suppression of thermal conductivity we reported previously for ZnO analogues of the present superlattices, and is in line with the results for the Zn-based hybrid from DEZ and HQ or ethylene glygol precursors of the type, *k*:*m* = 1:1 or *m*=0, with the present notation.[22-23] Note that, the present results demonstrate that in the ALD/MLD superlattices thermal conductivity can be systematically controlled by the superlattice period hence complementing the results of Refs. 22 and 23. Our recent results for the ZnO-based superlattices indicated that the phonon transmission through the molecular monolayers (from HQ) is actually hardly affected by the vibrational properties of the aromatic rings and that the suppression in thermal conductivity values is mainly due to the reduction in ZnO layer thickness, *i.e.*, the superlattice period.[34] This is consistent with the reduction in thermal conductivities for the present TiO_2-based superlattices. Regarding the possibilities to further suppress the thermal conductivity values obtained here, interesting questions concern, *e.g.*, the role of the organic layer thickness.

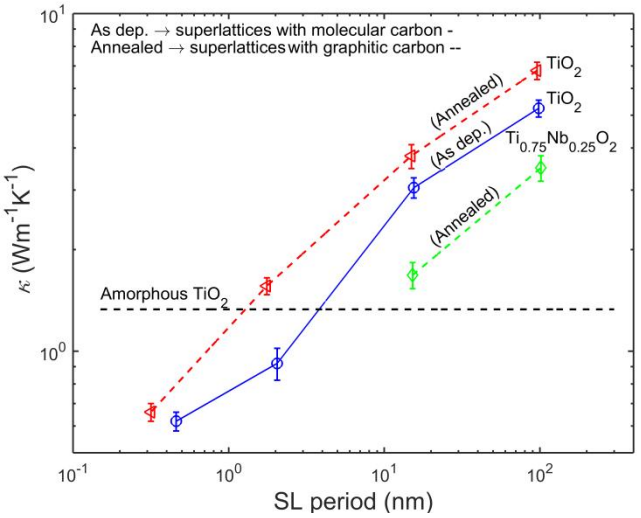

Figure 3 Thermal conductivity for the $[(TiO_2)_m(Ti\text{-}O\text{-}C_6H_4\text{-}O\text{-})_{k=1}]_n$ superlattice (SL) thin films for *k*:*m* ratio of 1:400 and 1:40, both as deposited and after annealing in Ar/H_2 gas at 600 °C; and for the annealed $[(Ti_{0.75}Nb_{0.25}O_2)_mC_{k=1}]_n$ with *k*:*m* = 1:400. Also shown are the thermal conductivities for the purely inorganic as-deposited TiO_2 film and for the annealed TiO_2 and $Ti_{0.75}Nb_{0.25}O_2$ films.

Conclusions

The cross-plane thermal conductivity in inorganic-organic TiO_2:C superlattices can be progressively hindered by decreasing the superlattice period - an effect that is mediated by incoherent boundary scattering at the sub-nanometer-thick graphitic layers within the TiO_2 matrix. In the present superlattices, we see a ten-fold decrease down to an ultra-low value of ~0.66 $Wm^{-1}K^{-1}$ - notably below the amorphous limit - for a superlattice period of ~0.3 nm. The TiO_2:C superlattices can be fabricated at first periodically confining molecular hydroquinone-based monolayers between thicker TiO_2 layer blocks by means of a self-limiting ALD/MLD technique, and then subsequently transforming the molecular layers into very thin graphitic layers via a reductive annealing treatment. It is of note that, by using such a fabrication route the number and the spacing of the thin graphitic layers is perfectly computer controlled and no transfer techniques are needed. Note also that, the present fabrication route is not limited to the TiO_2-organic material pair but is applicable to a wide library of materials that can be combined via the ALD/MLD chemistries to conformally coat a variety of three-dimensional nanostructures for future applications. Furthermore, tolerance to the employed high-temperature fabrication conditions indicates notable temperature stability for the present-kind superlattices and makes the structures attractive for high-temperature thermal barriers and thermoelectrics.

Acknowledgements

The present work has received funding from the European Research Council under the European Union's Seventh Framework Programme (FP/2007-2013)/ERC Advanced Grant Agreement (No. 339478) as well as the Aalto Energy Efficiency Research Programme and the United States Office of Naval Research (No. N00014-13-4-0528).

Notes and references

[1]Department of Chemistry, Aalto University, FI-00076 Aalto, Finland
[2]Department of Mechanical and Aerospace Engineering, University of Virginia, Charlottesville, Virginia 22904, USA
*Email: maarit.karppinen@aalto.fi

1W. S. Capinski, H. J. Maris, *Physica B*, 1996, **219&220**, 699-701.
2 G. Chen, *Phys. Rev. B*, 1998, **57(23)**, 14958-14973.
3 T. Yao, *Appl. Phys. Lett.*, 1987, **51**, 1798-1800.
4 G. Chen, *J. Heat Transf.* **1997**, 119(2), 220-229.
5 R. M. Costescu, D. G. Cahill, F. H. Fabreguette, Z. A. Sechrist, S. M. George, *Science*, 2004, **303**, 989-990.
6 C. Chiritescu, D. G. Cahill, N. Nguyen, D. Johnson, A. Bodapati, P. Keblinski, P. Zschack, *Science*, 2007, **315**, 351-353.
7 K. E. Goodson, *Science*, 2007, **315**, 342-343.
8 P. M. Norris, N. Q. Le, C. H. Baker, *J. Heat Transf.*, 2013, **135**, 061604-(1-13).
9 M. V. Simkin, G. D. Mahan *Phys. Rev. Lett.*, 2000, **84(5)**, 927-930.
10 J. Ravichandran, A. K. Yadav, R. Cheaito, P. B. Rossen, A. Soukiassian, S. J. Suresha, J. C. Duda, B. M. Foley, C.-H. Lee, Y. Zhu, A. W. Lichtenberger, J. E. Moore, D. A. Muller, D. G. Schlom, P. E. Hopkins, A. Majumdar, R. Ramesh, M. A. Zurbuchen, *Nature Mater.*, 2014, **13**, 168-172.
11 R. Y. Wang, R. A. Segalman, A. Majumdar, *Appl. Phys. Lett.*, 2006, **89**, 173113-(1-3).
12 P. J. O'Brien, S. Shenogin, J. Liu, P. K. Chow, D. Laurencin, P. H. Mutin, M. Yamaguchi, P. Keblinski, G. Ramanath, *Nature Mater.*, 2013, **12**, 118-122.
13 L. Hu, L. Zhang, M. Hu, J.-S. Wang, B. Li, P. Keblenski, *Phys. Rev. B*, 2010, **81**, 235427-(1-5).
14 W.-P. Hsieh, A. S. Lyons, E. Pop, P. Keblinski, G. D. Cahill, *Phys. Rev. B*, 2011, **84**, 184107-(1-5).
15 P. E. Hopkins, M. Baraket, E. V. Barnat, T. E. Beechem, S. P. Kearney, J. C. Duda, J. T. Robinson, S. G. Walton, *Nano Lett.*, 2012, **12**, 590-595.
16 P. Sundberg, M. Karppinen, *Beilstein J. Nanotechnol.*, 2014, **5**, 1104-1136.
17 K.-H. Yoon, K.-S. Han, M.-M. Sun, *Nanoscale Res. Lett.*, 2012, **7**, 71-(1-6).
18 T. Tynell, I. Terasaki, H. Yamauchi, M. Karppinen, *J. Mater. Chem. A*, 2013, **1**, 13619-13624.
19 J.-P. Niemelä, M. Karppinen, *Dalton Trans.*, 2015, **44**, 591-597.
20 M. Knez, K. Nielsch, L. Niinistö, *Adv. Mater.*, 2007, **19**, 3425-3438.
21 J. Malm, E. Sahramo, M. Karppinen, R. H. A. Ras, *Chem. Mater.*, 2010, **22**, 3349-3352.
22 J. Liu, B. Yoon, E. Kuhlmann, M. Tian, J. Zhu, S. M. George, Y.-C. Lee, R. Yang, *Nano Lett.*, 2013, **13**, 5594-5599.
23 T. Tynell, A. Giri, J. Gaskins, P. E. Hopkins, P. Mele, K. Miyazaki, M. Karppinen, *J. Mater. Chem. A*, 2014, **2**, 12150-12152.

24 Y. Furubayashi, T. Hitosugi, Y. Yamamoto, K. Inaba, G. Kinoda, Y. Hirose, T. Shimada, T. Hasegawa, *Appl. Phys. Lett.*, 2005, **86**, 252101-(1-3).
25 J. Jaćimović, R. Gaál, A. Magrez, J. Piatek, L. Forró, S. Nakao, Y. Hirose, T. Hasegava, *Appl. Phys. Lett.*, 2013, 102, 013901-(1-3).
26 J.-P. Niemelä, Y. Hirose, T. Hasegawa, M. Karppinen, *Appl. Phys. Lett.*, 2015, **106**, 042101-(1-4).
27 D. G. Cahill, *Rev. Sci. Instrum.*, 2004, **75(12)**, 5119–5122.
28 A. J. Schmidt, X. Chen, G. Chen, *Rev. Sci. Instrum.*, 2008, **79**, 114902-(1-9).
29 P. E. Hopkins, J. R. Serrano, L. M. Phinney, S. P. Kearney, T. W. Grasser, C. T. Harris, *J. Heat Transfer*, 2010, **132**, 081302-(1-10).
30 A. C. Ferrari, J. Robertson, *Phys. Rev. B*, 2000, **61(20)**, 14095-14107.
31 M. A. Pimenta, G. Dresselhaus, M. S. Dresselhaus, L. G. Cançado, A. Jorio, R. Saito, *Phys. Chem. Chem. Phys.*, 2007, **9**, 1276-1291.
32 A. I. Abdulagatov, K. E. Terauds, J. J. Travis, A. S. Cavanagh, R. Raj, S. M. George, *J. Phys. Chem. C*, 2013, **117**, 17442-17450.
33 C. Tasaki, N. Oka, T. Yagi, N. Taketoshi, T. Baba, T. Kamiyama, S. Nakamura, Y. Shigesato, *Jpn. J. Appl. Phys.*, 2012, **51**, 035802-(1-5).
34 A. Giri, T. Tynell, J.-P. Niemelä, J. Gaskins, B. F. Donovan, M. Karppinen, P. E. Hopkins, *Phys. Rev, Lett.*, 2015, (submitted).

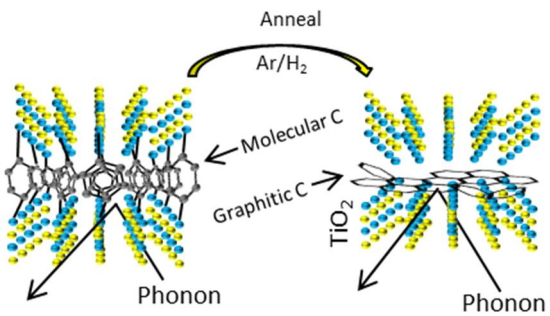

Table of contents Fig.

